AN INTERFEROMETRIC VIBRATION SENSOR BASED ON A FOUR- CORE OPTICAL FIBER

by

Belkıs Gökbulut

B.S., in Physics, Yeditepe University, 2012

Submitted to the Institute for Graduate Studies in
Science and Engineering in partial fullfilment of
The requirements for the degree of
Master of Science

Graduate Program in Physics

Boğaziçi University

2015

ACKNOWLEDGEMENTS

I would like to express my gratitude to my thesis supervisor Professor M. Naci İnci for all the encouragement, relieving guidance throughout my MSc thesis study and unending kindness, providing the opportunity to study at cooperative and productive atmosphere with him and engagement through the learning process of this master thesis.

I would like to extend my thanks to my laboratory colleagues, Miss Sema Güvenç, Miss Gülşen Kösoğlu and Mr Ekrem Yartaşı for their support, valuable suggestions and most importantly for their precious friendship during my studies.

I would like to express my gratitude to Boğaziçi University Research Fund for their support to this research project under Project Number BAP 10522.

Finally, I would like to thank my family, who have encouraged me for an academic career and supported me throughout the entire process of my education, both by keeping me motivated and confident. I will be grateful forever for their love and endless patience. My special thanks to my parents and my brother Mr Furkan Gökbulut for his support and contributions.

ABSTRACT

AN INTERFEROMETRIC VIBRATION SENSOR BASED ON A FOUR-CORE OPTICAL FIBER

In this thesis, an interferometric fiber optic vibration sensor based on a four-core optical fiber is described. When the light is coupled into the four cores, each core acts as a mutually coherent waveguide with the other ones, which allows obtaining an interference fringe pattern at the far field. Vibrating a section of the four-core optical fiber causes a path difference between the light beams guiding in the separate cores, which results in a shift in the fringe pattern. Such a mechanism allows one to relate the fringe shift to the vibration amplitude and frequency. In this study, a source, which is capable to generate 100 Hz frequency sound waves is attached to the optical fiber to maintain vibration of the section of the fiber. A single slit and a photodetector are used to detect the shifting of the fringe pattern that causes a change in the phase of the guiding light. When a He-Ne laser beam is coupled into the optical fiber, the structured fringe pattern is projected onto the slit behind the photodetector, then a small part of the fringe pattern is analysed. Thus, an interferometric fiber optic vibration sensor based on a four-core optical fiber, which has a simple structure and high sensitivity, is accomplished.

ÖZET

DÖRT ÇEKİRDEKLİ OPTİK FİBERE DAYANAN GİRİŞİM ÖLÇER TİTREŞİM SENSÖRÜ

Bu tezde, dört çekirdekli optik fiber esas alınarak, enterferometrik bir fiber optik titreşim sensörünün inşası üzerine çalışılmıştır. Işık dört çekirdeğin içine girdiğinde, her çekirdeğin diğer çekirdeklerle eş fazlı hareket etmesiyle, uzak bir alanda saçak girişim deseni meydana gelir. Dört çekirdekli optik fiberin bir parçasının titreştirilmesi, ayrı çekirdeklerde ilerleyen ışık hüzmeleri arasında yol farklılığı oluşturarak, saçak deseninin kaymasına neden olur. Böyle bir mekanizma, saçak kayması ile titreşimin genlik ve frekansı arasında ilişki kurulmasını sağlar. Bu çalışmada, fiberin bir kısmının titreşimini sağlamak için, 100 Hz frekansında ses dalgası üreten bir kaynak optik fibere bağlanmıştır. Işığın faz değişimine neden olan saçak deseninin kaymasını saptamak için, bir yarık ve fotodetektör kullanılmış, daha sonra saçak deseninin küçük bir parçası incelenmiştir. Böylece, dört çekirdekli optik fibere dayanan, girişim ölçer fiber optik titreşim sensörü başarıyla elde edilmiştir.

TABLE OF CONTENTS

LIST OF FIGURES

LIST OF SYMBOLS / ABBREVIATIONS

a	Radius of the fiber core
I	Intensity of light
I_r	Reflected irradiance
I_i	Incident irradiance
F	Finesse
k	Wave number
k_0	Wave number in free space
L	Fiber length
R	Surface reflectivity
n_0	Refractive index of air
n_1	Refractive index of the core
n_2	Refractive index of the cladding
NA	Numerical aperture
V	Mode number
λ	Free-space wavelength
Δ	Normalized index difference
θ	Illumination angle
θ_i	Incident angle
θ_t	Transmitted angle
θ_c	Critical angle
α_{max}	Maximum acceptance angle
δ	Separation distance between fiber cores

$\emptyset$	Phase difference
$\mathcal{E}$	Strain
FTP	Fourier Transform Profilometry
FPI	Fabry-Perot Interferometers
FFPI	In in-fiber Fabry Perot Interferometer
FBG	Fiber Bragg grating

1. INTRODUCTION

Vibration detection is an important issue for industrial processes to predict maintenance. Many techniques have been used to detect the vibration amplitudes. However, in environments that is exposed to electrical signals, it is difficult to detect the physical parameters properly; usually due to electromagnetic interference. Therefore, there has been a significant rise of interest in employing optical fiber sensors with the ability to eliminate the effects of the electromagnetic interference in such harsh environments. In contrast with the conventional ones, optical fiber sensors can be applied in noisy environments with a high level of electromagnetic radiation. Such optical sensors have also small sizes, light weight, high temperature performance, high sensitivity, large bandwidths [1].

Over the last two decades, fiber optic technology has been enhanced to measure various physical parameters like strain, vibration, temperature, pressure, humidity in harsh environments and remote locations [2-10]. Beside, using an optical fiber as a medium to transmit information, the properties of light wave in an optical fiber, like intensity and phase modulations, are used for sensor technologies. The advantages of the fiber optic sensors make them attractive in various applications used in industrial processes; such as quality control systems and medical diagnostics are to mention a few of them [11]. Also, some fiber optic sensors provide observing real time abnormalities of bridges, constructions and aircrafts [12].

There are mainly two types of optical fiber sensors: intensiometric and interferometric ones. Since the intensiometric sensors depend on the power of the light source, significant errors occur if the intensity of light is weak or something affects to the source intensity. In contrast, interferometric sensors, which depend on observed interference patterns, are much more accurate. Therefore, many types of the interferometric sensors such as Fiber Bragg Grating sensors, Fabry-Perot [13] and Mach-Zender [14] interferometers have been improved and employed in various scientific and industrial applications during the last decades.

Fiber optic interferometric sensors are mainly based on the interference of two light beams propagating through different optical paths of a single fiber or two different fibers.

After one of the optical paths, which is exposed to external perturbations, for example, say one arm of the Mach-Zhender interferometer, the device in concern emits a signal, which is directly related to the effects of the external perturbations. The perturbation induced variations in the interferometer's signal are detected through monitoring wavelength shifts, phase change, intensity fluctuations, frequency variations or changes in the bandwidth of the signals [15].

Beside the advantages of the interferometric fiber optic sensors, generally they have complex structures that lead to difficulties in fabrication and high cost, while also decreasing the reliability of the sensor. In other respects, the resolution of the interferometric fiber optic sensors highly depends on the resolution of spectrometers used in the experimental setups. Avoiding complex structures and costly equipment such as spectrum analyzers, interferometric fiber optic sensors, which are mainly based on the intrinsic properties of optical fiber material itself, have come to the attention of researchers over the last two decades. These sensors' working mechanism is generally based on the interference of two light beams propagating either in one, two or multi-core optical fibers [16,17].

The cores of the multi-core optical fiber used in our work behave as different arms of an interferometric sensor such as Mach-Zehnder or Michelson interferometer. When light is coupled into the cores of the fiber, each core acts as a mutually coherent waveguide with the other cores, which allows obtaining an interference fringe pattern at the far field. The external parameters lead to a change in the optical paths of light beams in each core, which results in a phase difference.

Multicore fibers used in our work were used before in various sensing applications, for example, as bending sensor and as interferogram source for non-invasive optical profilometric applications for three dimensional surface topography measurements.

In this thesis research, a four-core optical fiber is used for the first time to construct a fiber optic vibration sensor. Vibrating a section of the four core optical fiber causes a path difference between the light beams guiding in separate cores, which results in a shift in the fringe pattern. Such a mechanism allows one to relate the fringe shift to the amplitude and

frequency of the vibration. Thus, an interferometric fiber optic vibration sensor based on a four-core optical fiber, which has a simple structure and high sensitivity, is accomplished.

This thesis consists of four chapters: The first chapter provides an introduction of fiber optic sensors and multi-core optical fibers and summarizes some advantages of vibration sensing based on four core optical fiber which indicates why this type of sensor is preferred over conventional sensors.

The second chapter present a brief review of theoretical background of multi-core optical fibers and using a multi-core fiber as bending sensor. In addition, this chapter gives some basic information about vibration sensors based on optical fibers such as Fabry-Perot Interferometer and Fiber-Bragg Gratings.

In the third chapter of the thesis, the theory of bending based on multi-core optical fiber is explained; which is followed by the experimental setup, results and discussion. The signals corresponding to the light intensity, which indicates vibration amplitude and frequency, are analyzed using data from graphs. Vibration parameters relating the vibration amplitude and vibration frequency to the change in phase of the guiding monochromatic laser light are demonstrated. In addition, this chapter gives some information about which problems we come across in the experimental setup and how to overcome these problems.

In the last chapter of the thesis, measures taken to construct a well performing vibration sensor based on the four-core optical fiber and the difficulties encountered in the system are discussed. Furthermore, the arguments which signify how to improve the system’s quality and the suggestions for future work are given.

2. REVIEW

2.1 General Outline

There are varieties of fiber optic sensors that can be classified into three categories in terms of their sensing features, employing the intrinsic properties of the optical fiber itself and point or distributed fiber optic sensors. According to their sensing features, optical sensors are classified as intensity sensors and interferometric sensors. While intensity sensors detect the intensity variations of light during the sensing process, interferometric sensors determine the phase-induced changes from optical path differences of light beams. Another classification, which is related to the using of the fiber is called extrinsic or intrinsic sensors. In intrinsic sensors, physical properties of the fiber such as changes in the refractive index and length when an external parameter like strain/temperature is present. In extrinsic sensors, a fiber is used only to transmit a signal of light to a sensing region. Finally, fiber optic sensors are classified as distributed and point sensors based on their measurement points. While distributed sensors have ability to sense any point along a fiber, the point sensors provide only a single measurement point along the fiber [11].

2.2 Optical Fibers

An optical fiber is a cylindrical waveguide having a central core where light is coupled into, which is covered by a cladding of lower refractive index material than the core of the fiber shown in Figure 2.1 [18]. Optical fibers are categorized based on the refractive index profile and mode numbers.

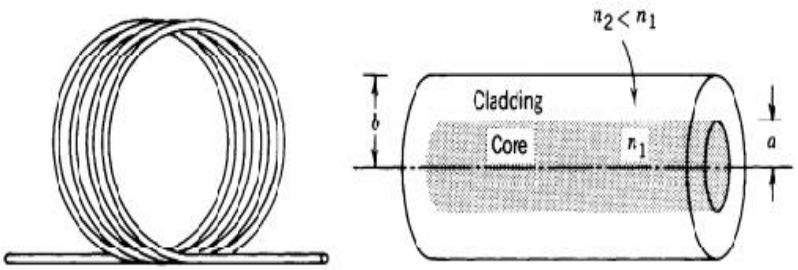

Figure 2.1. A step-index optical fiber [18].

According to the refractive index profile, optical fibers are identified as step-index or graded-index fibers. For the step index fiber, the refractive indices of the core and the cladding are constant along their boundaries (see Figure 2.2a and b). Whereas for the graded index fiber, the refractive index of the fiber core changes from a maximum value at its center to a minimum value at the core-cladding boundary (See Figure 2.2c) [18].

In terms of the mode numbers, optical fibers are also described as single-mode and multi-mode fibers. A single mode fiber, which has a small core diameter allows only a fundamental mode to propagate through the fiber as shown in Figure 2.2b. Multimode fibers with large core diameters allow light to propagate through various modes as shown in Figure 2.2a.

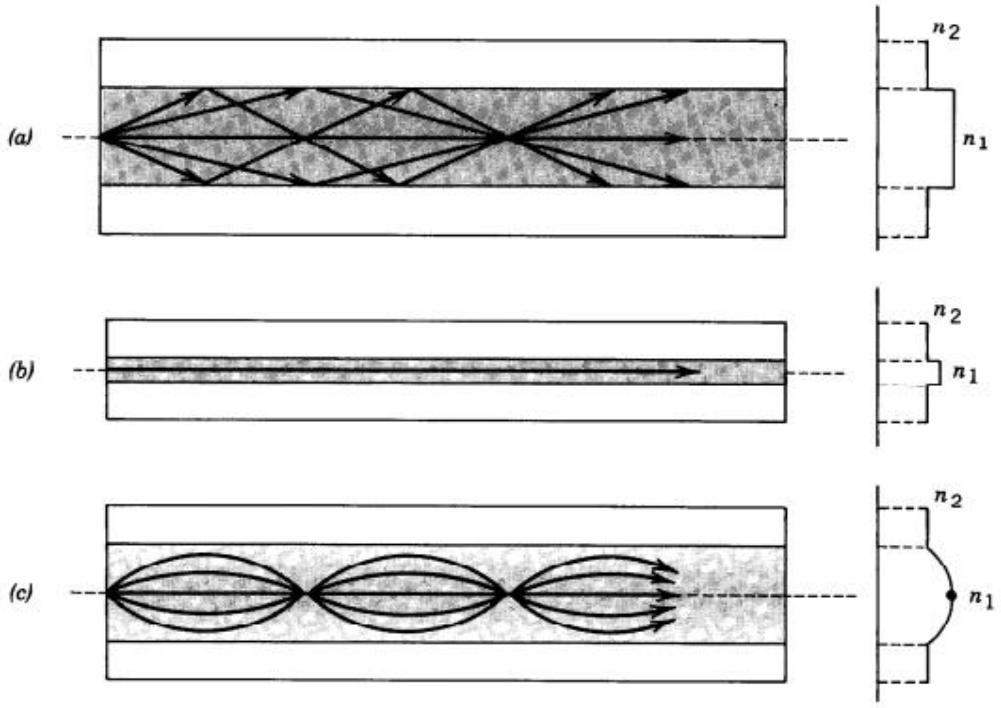

Figure 2.2. Refractive index profile for (a) a multimode step-index fiber, (b) a single mode step index fiber, and (c) a multimode graded index fiber [18].

In a step index fiber, *V*- number defines the number of modes in a fiber that is given by [19]:

$$V = \frac{2\pi a}{\lambda}(n_1{}^2 - n_2{}^2)^{1/2} \tag{2.1}$$

$$V = \frac{2\pi a}{\lambda}(2n_1 n\Delta)^{1/2} \tag{2.2}$$

where a is the radius of the fiber core, n is the average refractive index of the core and cladding, λ is the free-space wavelength, and Δ is the normalized index difference given by

$$\Delta = \frac{n_1 - n_2}{n_1} \tag{2.3}$$

When the *V*-number is smaller than 2.405, a single-mode fiber can be designed. Otherwise, as the *V*- number exceeds 2.405, a multimode optical fiber which allow higher modes to propagate through the fiber is obtained.

The propagation of light in optical fibers is based on the principle of the total internal reflection of an optical waveguide as explained in the following section.

2.2.1. Total Internal Reflection

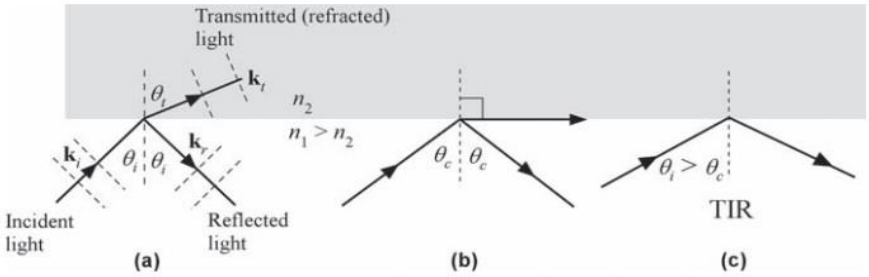

Figure 2.3. Representation of critical angle and total internal reflection [19].

When light wave propagates from a dielectric medium-1 of refractive index n_1 towards a medium-2 of a smaller refractive index n_2, a part of the ray is reflected and the rest is transmitted. The transmitted wave is called as refractive light. It is obviously shown in Figure 2.3a. that the transmitted angle θ_t is greater than the incident angle θ_i,

The refraction angle is related to the properties of two media. The relationship is known as the *Snell's law* and is given by [20],

$$n_1 \sin\theta_i = n_2 \sin\theta_t \tag{2.4}$$

When the incident light propagates at some specific angle Θ_c, which is called the critical angle, the refracted ray propagates parallel to the boundary interface. Therefore Θ_t becomes equal to 90° and the critical angle is given by,

$$\sin\theta_c = \frac{n_2}{n_1} \tag{2.5}$$

When the incident angle is greater than the critical angle, there will be only reflected light. The phenomenon is called the Total Internal Reflection (TIR). A light ray propagating through an optical fiber is based on the Total Internal Reflection principle. The effect of the increasing angle and the acceptance angle of the optical fiber is explained in the next chapter.

2.2.2. Numerical Aperture

In an optical fiber, only rays falling within a certain cone can propagate, not all light waves can. Figure 2.4 demonstrates the optical path of on incident light wave from outside medium of refractive index n_0 to the fiber core of refractive index n_1.

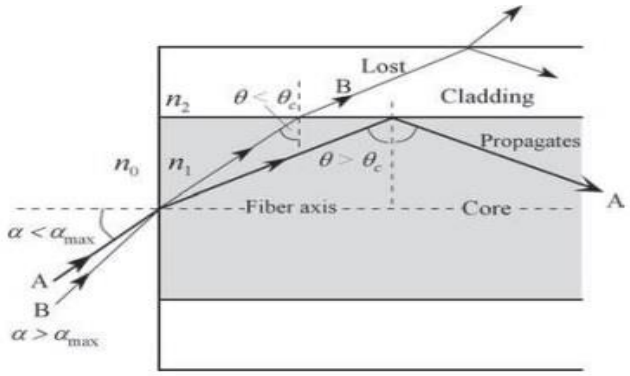

Figure 2.4. Representation of the acceptance angle α [14].

The incidence ray penetrates at the end of the fiber core with an angle α and the ray makes an angle θ with the normal to the boundary interface between fiber core of refractive index n_1 and cladding of refractive index n_2. When the angle θ is less than the critical angle θ_c, the ray escapes to into the cladding. To provide total internal reflection, incident angle reaches its maximum value, which is called the *acceptance angle* α_{max} for $\theta = \theta_c$.

At the n_0- n_1 interface, Snell's law gives [21],

$$\frac{\sin \alpha_{max}}{\sin\left(\frac{\pi}{2} - \theta_c\right)} = \frac{n_1}{n_0} \tag{2.6}$$

$$\sin \alpha_{max} = \frac{n_1}{n_0} \cos \theta_c \tag{2.7}$$

$$\sin \alpha_{max} = \frac{n_1}{n_0} (1 - \sin^2 \theta_c) \tag{2.8}$$

To eliminate θ_c, Eq. 2.5 is inserted into Eq. 2.8,

$$\text{Sin}\, \alpha_{max} = \frac{({n_1}^2 - {n_2}^2)}{n_0} \tag{2.9}$$

The *numerical aperture NA* is a characteristic parameter of an optical fiber determined by

$$NA = ({n_1}^2 - {n_2}^2) \tag{2.10}$$

In terms of NA, maximum acceptance angle α_{max} is described by

$$\text{Sin}\, \alpha_{max} = \frac{NA}{n_0} \tag{2.11}$$

2.2.3. Two-core Optical Fibers

A schematic illustration of a two-core optical fiber is shown in Figure 2.5. When the light is coupled into two cores of the optical fiber, two mutually coherent beams that move across the separate cores occur.

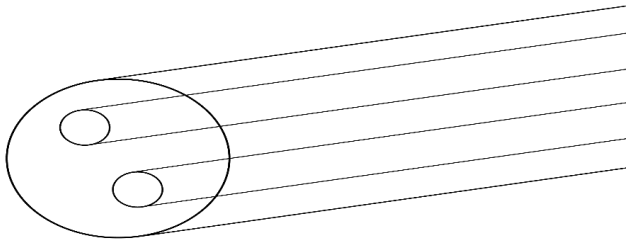

Figure 2.5. A two-core optical fiber

Two cores behave like double slits in that of the Young double slit experiment. In the Young double slit experiment, when two parallel slits, S_1 and S_2 separated by a distance s are illuminated by a common laser beam, waves emitting from the slits interfere at a screen far away from the slits to form a fringe pattern shown in the Figure 2.6. The fringe pattern, which is called the *Young's Interference fringes*, is formed by dark and light lines that refer to maximum and minimum intensities.

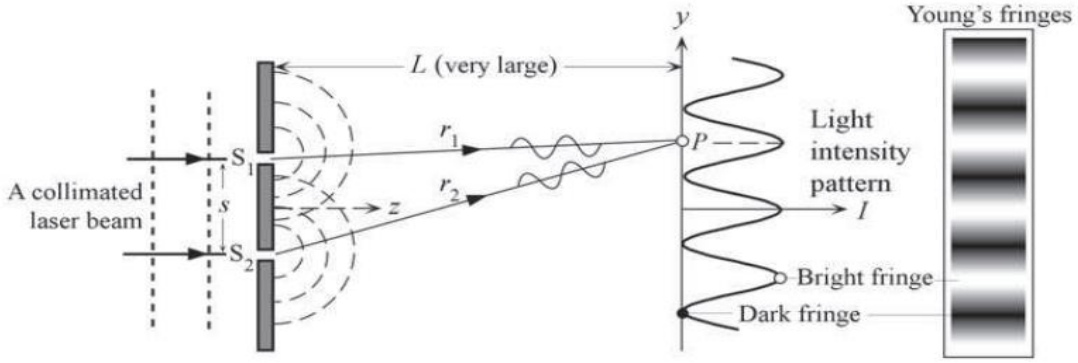

Figure 2.6.Young double slit experiment [19]

Since two slits are illuminated by the same laser beam, they emanate coherent light beams, which have equal irradiances. As the beams have different optical paths, there is a phase difference between the waveguides.

The phase difference ∅ at point P with a distance y on the screen is given by [19];

$$\emptyset = k(r_2 - r_1) \tag{2.12}$$

The intensity at point P is,

$$I = I_1 + I_2 \tag{2.13}$$

$$I = I_0(1 + \cos[\emptyset]) \tag{2.14}$$

Maxima occur for the phase value of $\emptyset = 2m\pi$ and minima occur for the phase $\emptyset = (2m+1)\pi$, where $m = 1,2,3\ldots$

If *L*, which refers to the distance between screen and slits, is far away from the slits, the approximation is given by

$$(r_2 - r_1) \cong \left(\frac{S}{L}\right) y \tag{2.15}$$

Therefore, the irradiance from the slits becomes

$$I = I_0 \left(1 + \cos\left[\left(\frac{S}{L}\right) ky\right]\right) \tag{2.16}$$

When a laser beam is coupled into the two cores of the optical fiber, the results will be the same as that of the Young double slit experiment.

2.2.4. Four-Core Optical Fibers

A schematic illustration of a four-core optical fiber is shown in Figure 2.7.

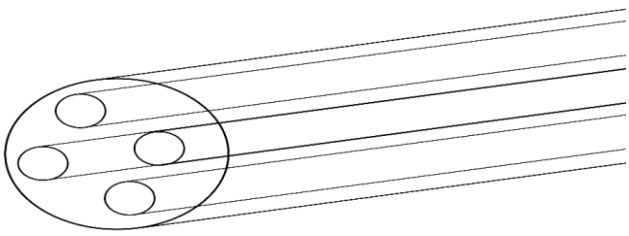

Figure 2.7. A four core optical fiber

When a light beam is coupled into a four-core optical fiber, each core of the fiber acts as an independent waveguide to interfere at the far field, that is, at a point *P*(x, y), which is shown in Figure 2.8.

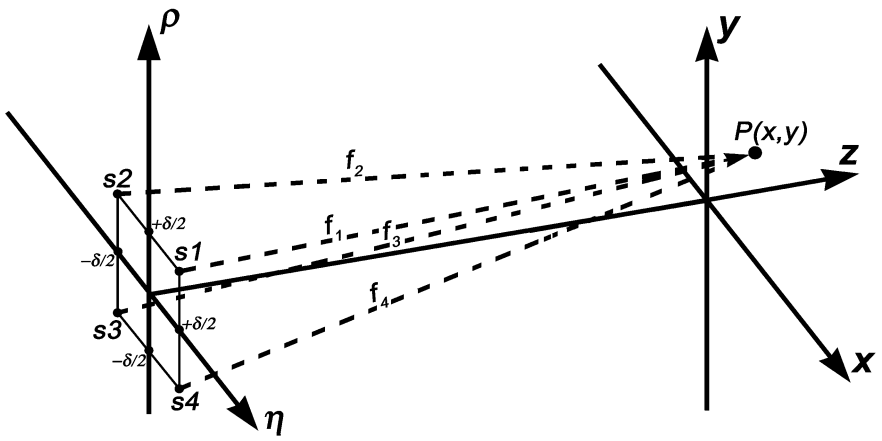

Figure 2.8. A schematic illustration of a geometry of four point source and the interference point, P(x,y) [22].

There are four different interferograms generated by six couplings of the fiber cores, which are shown in Figure 2.9. A vertical interferogram is formed by pairings of the horizontal cores, a horizontal interferogram is formed by pairings of the vertical cores and the pairings of the diagonal cores produce two opposite diagonal interferograms.

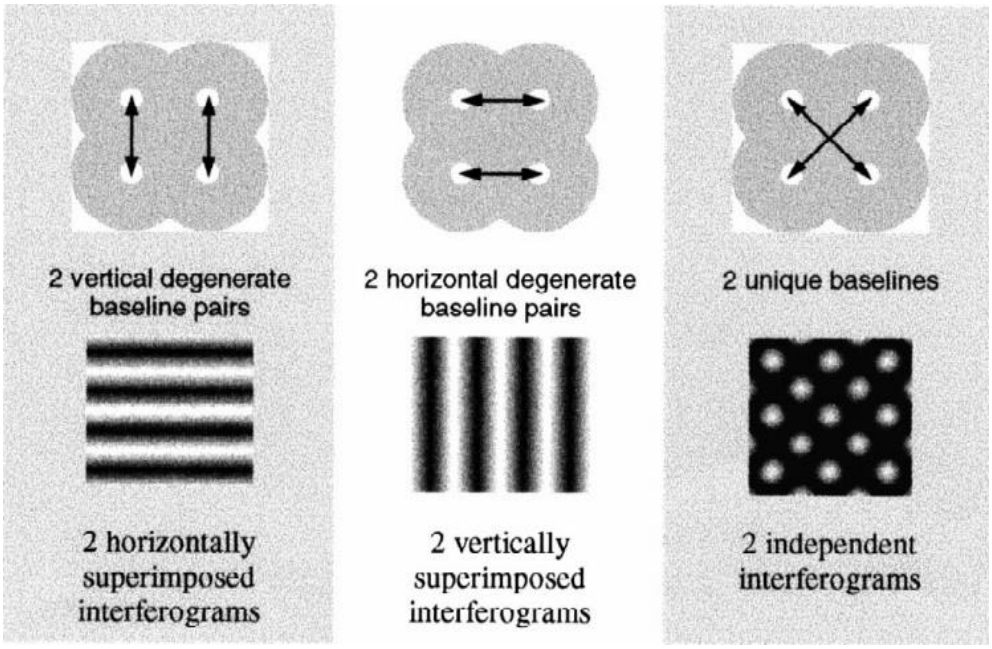

Figure 2.9. The interferogram produced from four-core optical fiber [17]

The superposition of these interferograms enables an interferometric fringe pattern shown in Figure 2.10.

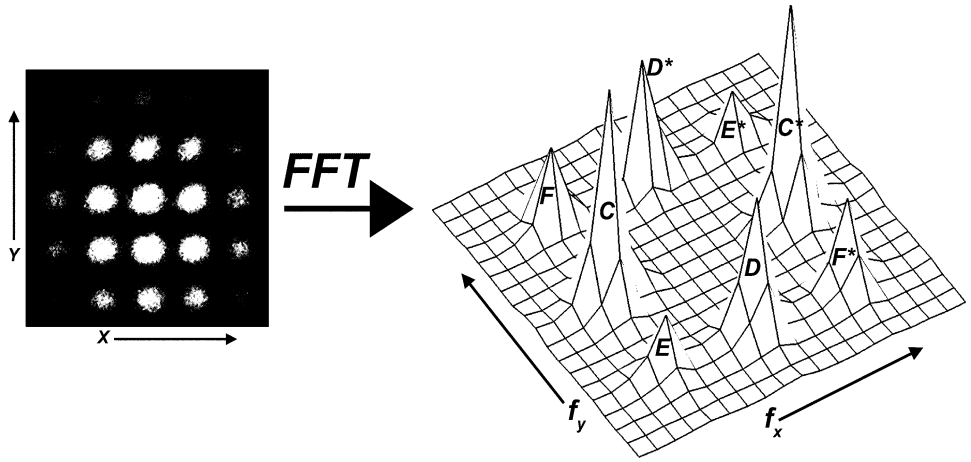

Figure 2.10. A fringe pattern from a four core optical fiber and its 2-D Fourier spectrum [22].

The intensity of the fringe pattern produced from four core optical fiber is given by [22],

$$I(x,y) = 2I_O \begin{bmatrix} 2 + 2\ \cos\left(2\pi\frac{\delta}{\lambda f}(x\cos\theta - z(x,y)\sin\theta)\right) \\ +2\cos\left(2\pi\frac{\delta}{\lambda f}(y\cos\theta - z(x,y)\sin\theta)\right) \\ +\cos\left(2\pi\frac{\delta}{\lambda f}((x+y)\cos\theta - z(x,y)\sin\theta)\right) \\ +\cos\left(2\pi\frac{\delta}{\lambda f}((x-y)\cos\theta - z(x,y)\sin\theta)\right) \end{bmatrix} \quad (2.17)$$

where θ is the illumination angle, λ is the wavelength of the light beam, δ is the separation distance between the cores and x, y, z are the coordinates of the interferogram, but in this work, there is no height of the fringe pattern and the cores are illuminated by the laser at zero degree angle.

Therefore, when z=0 and θ=0, the intensity equation become;

$$I(x,y) = 2I_O \begin{bmatrix} 2 + 2\cos\left(2\pi \frac{\delta}{\lambda f}(x)\right) \\ +2\cos\left(2\pi \frac{\delta}{\lambda f}(y)\right) \\ +\cos\left(2\pi \frac{\delta}{\lambda f}((x+y))\right) \\ \cos\left(2\pi \frac{\delta}{\lambda f}((x-y))\right) \end{bmatrix} \quad (2.18)$$

A four core optical fiber was employed in the scientific literature before for two-axis bend measurements, 3D surface profilometry and vibration amplitude analysis of 3-D vibrating objects.

2.3. Using a Multi-Core fiber as Bending sensor

As stated above, four core optical fiber was used by Gander et al [17] for the first time to measure two axis bending. When the light is coupled into two cores of the optical fiber, multicore optical fiber acts as two arms in a Mach-Zehnder Interferometer. Light is split into two mutually coherent beams that move across the separate cores. Therefore a fringe pattern emerges at the far field as explained in the previous chapter and bending causes a shift in the fringe pattern.

Bending of the fiber form a curvature with radius *R* causing a difference in strain between the cores, which are considered as independent strain gauges as shown in Figure 2.11.

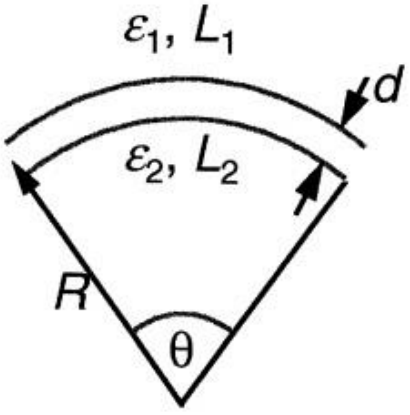

Figure 2.11. Bending of the fiber [17].

When the separation distance between the cores is *d* and unstrained length of the fiber is *L*, a variation in the strain between the cores can be calculated as

$$\Delta\varepsilon = \frac{d}{R} = \left(\frac{d}{L}\right)\Delta\theta \tag{2.19}$$

where $q = \frac{L}{R}$ is the bending angle

The phase change of the light due to the bending induced strain is given by [17]

$$\Delta\emptyset \approx \frac{2\pi L}{\lambda}\left(n + \frac{dn}{d\varepsilon}\right)\Delta\varepsilon \tag{2.20}$$

Interferometric fiber optic bending/nano-displacement sensor was also studied using a plastic dual-core optical fiber by H.Qu et al [16]. Bending of the fiber in x-z plane leads to a strain between two cores, which makes variations both in refractive index due to photo elastic effect and the lengths of the two cores. The displacement *d* of the fiber creates changes in the phase of light beams in each cores. The variations of phase difference can be calculated as [16],

$$\delta\emptyset \approx 2k_0[(l\delta n_1 + n\delta l_1) - (l\delta n_2 + n\delta l_2)] \tag{2.21}$$

$$\delta\emptyset \approx 2k_0 nl[(\delta n_1 - \delta n_2)/n + (\delta l_1 - \delta l_2)/l] \tag{2.22}$$

where δl_1, δl_2 are length changes of the cores 1 and 2 and δn_1, δn_2 are refractive indices changes of the cores 1 and 2, k_0 is the wave-number.

The difference in strain between two cores can be expressed as;

$$(\delta l_1 - \delta l_2)/l = \Lambda/R \tag{2.23}$$

where *R* is the bending radius and Λ is the distance between the cores.

The difference in the refractive index due to bending of the two cores can be described as [23]

$$(\delta n_1 - \delta n_2)/n = C\Lambda n^2/R \tag{2.24}$$

C is a constant, which is related to the photo elastic tensors of the core material. When Eq. 2.23 and 2.24 are inserted into Eq. 2.22,

$$\delta\emptyset = 4\pi n(1 + Cn^2)\left(\frac{l}{R}\right)\left(\frac{\Lambda}{\lambda}\right) \tag{2.25}$$

Using an approximation, which assumes that the displacement *d* of the fiber tip is much smaller than the fiber length *l*, the bending radius can be calculated as

$$R = l^2/2d \tag{2.26}$$

When the approximated radius is inserted into Eq. 2.25, the phase difference become [16],

$$\delta\emptyset = 8\pi n(1 + Cn^2)\left(\frac{d}{l}\right)\left(\frac{\Lambda}{\lambda}\right) \tag{2.27}$$

2.4 Using a Multi-Core fiber for Optical profilometry

A four core optical fiber was used for an optical profilometry system to measure 3-D rigid body shapes. FTP technique was applied to process grating light pattern produced by interference of four wave fronts emitted from the fiber cores. The fringe pattern, which is projected onto an object surface, includes information of the object's surface topography. The images, which are captured by a CCD camera, were analyzed Fourier transform profilometry [22].

A structured light pattern of the four core optical fiber was also used to analyze vibration amplitude with taking a single frame of a vibrating object using a CCD camera. FTP technique was used to process light pattern projected onto the vibrating objects [24].

2.5 Optical fibers as Vibration Sensors

2.5.1. Fabry-Perot Interferometer

Fabry-Perot Interferometers are based on multiple-beam interference in a cavity, which is composed of a space between two semi-reflective mirrors. Multiple reflections in a Fabry-Perot cavity cause interferometric fringes. When the cavity is exposed to some external disturbances, phase change causing a variation in the fringe pattern occur. This principle maybe used to construct optical vibration sensors [13, 25].

The phase-delay in the cavity is given by [18] as

$$\emptyset = \frac{2\pi(2ndcos\theta)}{\lambda} \tag{2.28}$$

where n is the refractive index of the medium, d is the separation between mirrors, θ is the angle of incidence and λ is the wavelength through propagation.

The ratio between reflected irradiance I_r and incident irradiance I_i is cyclic with the round trip phase difference between beams shown in [1]

$$\frac{I_r}{I_i} = \frac{F\sin^2(\emptyset/2)}{1 + F\sin^2(\emptyset/2)} \tag{2.29}$$

$$F = \frac{4R}{(1-R)^2} \tag{2.30}$$

where, F is the finesse of the cavity, R is the surface reflectivity of the cavity and $\emptyset$ is the phase difference between the traversing beams.

In in-fiber Fabry Perot Interferometer (FFPI), the partial mirror surfaces are inside the fiber that means both end of the fiber has a partially transmitting mirror to form the fiber Fabry-Perot cavity. The FFPI vibration sensing configuration is demonstrated in Figure 2.12.

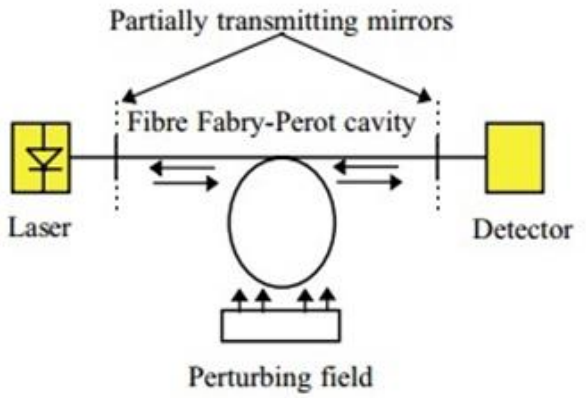

Figure 2.12. FFPI sensor [13]

2.5.2. In-Fiber Bragg Grating (FBGs) Interferometer

FBGs sensors are based on a series of partial reflectors prepared with a determined spatial period. The periodic variations of the refractive index of the core of an optical fiber allow obtaining such reflectors. In the FBG sensor structure, only certain wavelengths based on the refractive index profile shown in Figure 2.13 are reflected; thus the structure behaves as a wavelength selective reflector. The changes in the optical properties of the fiber allow one to use these devices for optical sensing applications such as temperature and strain sensors [26, 27].

In vibration sensing applications, vibration induce strain variations, which lead to resonance of the FBG wavelength, and hence observing of the resonance allows measuring those vibration parameters [28].

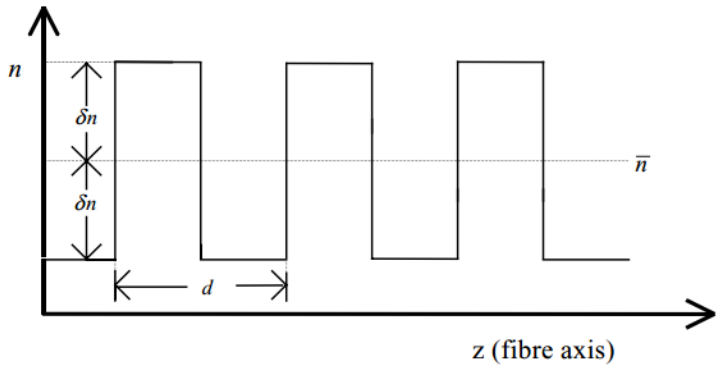

Figure 2.13. Refractive index profile of an FBG [13]

Fabry-Perot Interferometer (FPI) with fiber Bragg grating mirrors (FBG) is also used for vibration sensing. FPI-FBG sensor is demonstrated in Figure 2.14.

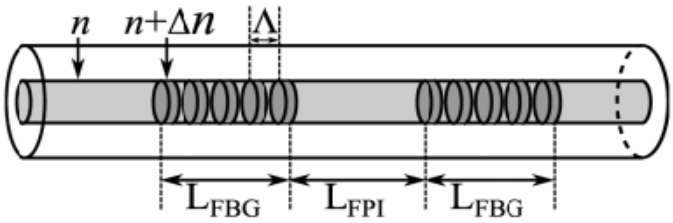

Figure 2.14. FPI-FBG sensor [29]

For this type of sensors, mechanical vibrations result in a change in the Bragg wavelength due to strain induced variations in the length and refractive index of the FBG; therefore, the changes cause a shift in the peak within the reflection spectrum of the FBG. An optical spectrum analyzer is used to observe the reflectance spectrum and monitor the amount of the shifting [29].

2.5.3. Vibration Sensor using Multi-mode Optical Fiber

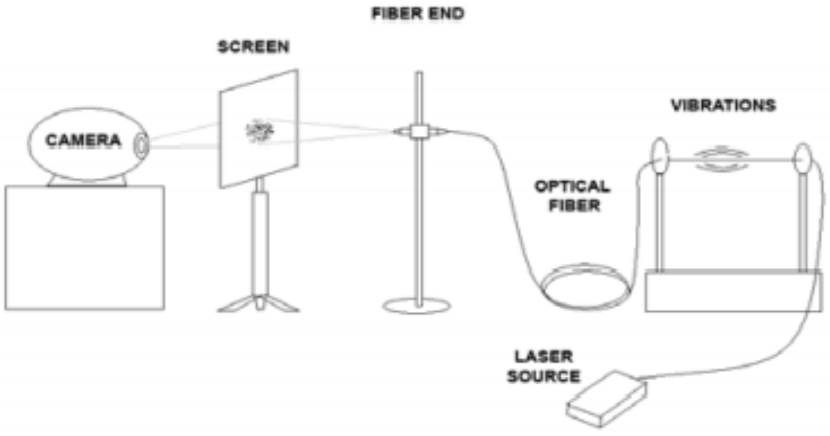

Figure 2.15. Basic sensor system for sensing vibration [30].

Vibration and their parameters are also detected by observing the mode distribution in a multi-mode optical fiber by Lujo et. al. [30]. A multi-mode fiber used in the experiment

has about 500 modes which have their own group velocities and propagation constants. The modes interfere with each other when they travel in the same medium [18].

In the experiment, a pattern formed due to interference of the modes from the fiber end is projected onto a screen. When various forces are applied to the fiber, variations occur in the propagation of the modes, which cause changes in their interference. Thus, the intensity distribution of the modes results in a change in the pattern at the fiber end. The system is shown in Figure. 2.15.

The output signal from the fiber, which signifies the changes in the intensity distribution, is detected by a video signal using a CCD camera. Figure 2.16 shows the difference between two sequent frames when the vibration is applied to the multi-mode optical fiber [30].

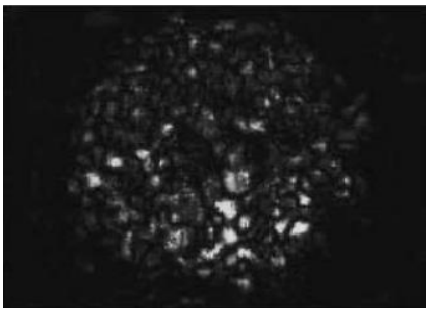

Figure 2.16. Difference between consecutive frames as multi-mode fiber is vibrating [30].

When the vibration is not applied to the multi-mode optical fiber, there is no difference between the two sequent frames. Consecutive frames are analyzed using MATLAB to demonstrate the intensity changes of the light pattern, which results in the detection of the vibration parameters.

In this thesis work, a four core optical fiber is employed for sensing frequency and amplitude of a vibrating object. When the vibration is applied to the optical fiber, the refractive index and length of the four-core fiber change, which introduce a phase difference between the light propagating in each fiber core. This type of an optical fiber sensor falls into an intrinsic sensor category. Furthermore, since an interferometric fringe pattern produced from the four core optical fiber is used to detect the variations of the path

differences of the guided rays in the cores, the optical sensor is also classified as interferometric sensor in terms of the sensing feature. Finally, vibration is applied at only a single point along the fiber, therefore, the sensor is also classified as point sensor according to the measurement point. The details on construction of the fiber sensor and measurement details are given in the following chapter.

3. EXPERIMENTAL WORK AND RESULTS

3.1 Theory

The principles of bend sensing based on multi-core optical fiber was studied by P. M. Blanchard et all [31]. When the optical fiber is bent, a strain between the cores causes an optical phase difference ($\Delta\emptyset$) between guiding light beams in the cores. The interferometric measurements of the phase difference allow using multi-core fibers in the area of bend sensing.

The rate of optical phase difference corresponding to the variations of the fiber refractive index (n) and the fiber length (L) with strain ($\mathcal{E}$) is given by [31]

$$\frac{\partial\phi}{\partial\varepsilon} = \frac{2\pi}{\lambda}\left(n(\varepsilon)\frac{\partial L(\varepsilon)}{\partial\varepsilon} + L(\varepsilon)\frac{\partial n(\varepsilon)}{\partial\varepsilon}\right) \tag{3.1}$$

where

$$L(\varepsilon) = L(1+\varepsilon) \tag{3.2}$$

is the sensor length which is exposed to bending

$$n(\varepsilon) = n - \varepsilon K n^3 \tag{3.3}$$

is refractive index of the fiber [32].

When Eq. 3.1-3.3 are combined;

$$\frac{\partial\phi}{\partial\varepsilon} = \frac{2\pi}{\lambda}\left((n-\varepsilon K n^3)\frac{\partial}{\partial\varepsilon}L(1+\varepsilon) + L(1+\varepsilon)\frac{\partial}{\partial\varepsilon}(n-\varepsilon K n^3)\right) \tag{3.4}$$

$$\frac{\partial \phi}{\partial \varepsilon} = \frac{2\pi}{\lambda}\left((n - \varepsilon K n^3)L + L(1+\varepsilon)(-Kn^3)\right) \tag{3.5}$$

$$\frac{\partial \phi}{\partial \varepsilon} = \frac{2\pi}{\lambda}(nL - \varepsilon K n^3 L - K n^3 L - K n^3 L \varepsilon) \tag{3.6}$$

$$\frac{\partial \phi}{\partial \varepsilon} = \frac{2\pi}{\lambda}(nL - 2\varepsilon K n^3 L - K n^3 L) \tag{3.7}$$

When a small second term is neglected, the phase difference between two fiber cores corresponding to their difference in length (ΔL) is given by [31]

$$\Delta\phi = \frac{2\pi}{\lambda}\Delta L(n - Kn^3) \tag{3.8}$$

In our experiments, fused silica at a wavelength of 633 nm with n = 1.46 and K = 0.103 [33] is used. When the two cores are separated by a distance δ and the fiber bending is along the arc of a circle with radius R through an angle ψ, the path difference between the cores is given by $\psi\delta$. When the values are put into Equation (3.8),

$$\Delta\phi = \frac{2\pi}{\lambda}\psi\delta(1{,}46 - 0{,}103\,.\,1{,}46^3) \tag{3.9}$$

Then, the optical phase difference becomes,

$$\Delta\phi = 1.14\frac{2\pi\delta}{\lambda}\psi \tag{3.10}$$

Figure 3.1 shows a schematic representation of a bending fiber along the arc of a circle. In our experiments, a strain due to vibration is applied to the point at the center of the stretched fiber with length 12 cm. The core separation of the fiber (δ) used in the experiment is equal to 40,6 μm; thus, according to Equation (3.10), when the phase change due to a strain is equal to π,

$$\pi = 1.14\frac{2\pi\ 40{,}6 \times 10^{-6}m}{633 \times 10^{-9}m}\psi \tag{3.11}$$

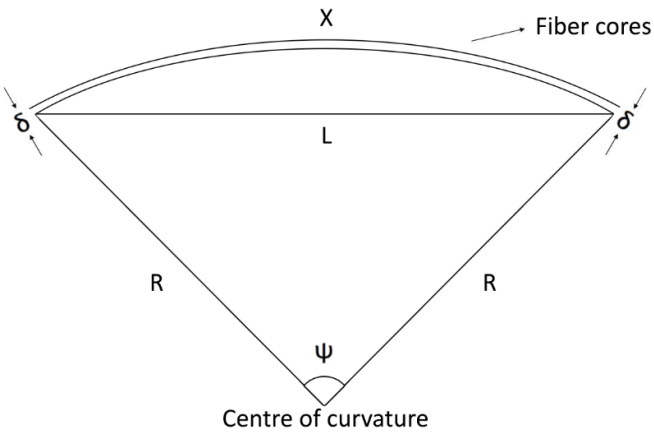

Figure 3.1. The representation of bending fiber

the bending angle ψ, will be approximately 0,3918 degrees.

To find the length of the bending fiber, firstly the radius of the curvature is found by applying Cosine Theorem to Figure 3.1.

$$12^2 = 2R^2 - 2R^2\cos(0{,}3918) \tag{3.12}$$

$$144 = 4{,}6760 \times 10^{-5}R^2 \tag{3.13}$$

The radius of the curvature, is determined to be approximately 17,549 m. Since the bending angle and the radius of the curvature are found, the length of the curvature is described using the geometric relation given by

$$R = \frac{x}{\psi} \tag{3.14}$$

The length of the bended fiber x, becomes nearly a length of 12,0018 cm, which means that the length of the fiber is increased by an amount of 1,8 μm when the vibration is applied.

3.2 Experimental Setup for Vibration Sensor

In the experiment, a four core optical fiber is used. The cross-sectional area of the four core fiber is seen Figure 3.2 [22]. Four cores are embedded in a single cladding with thickness 125 μm. The air holes which have one rectangular and four triangular shapes are due to manufacturing process. The length of the fiber used in the experiment is nearly 40 cm. Distance between adjacent cores is 40,6 μm, and each core diameter is 10,6 μm.

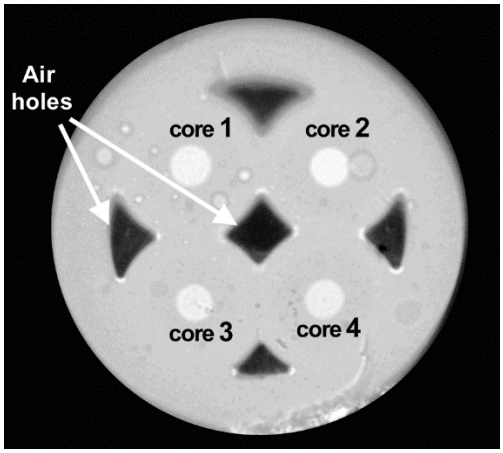

Figure 3.2.The cross sectional area of the four-core fiber

The experimental setup of the vibration sensor based on a four-core optical fiber is shown in Figure 3.3.

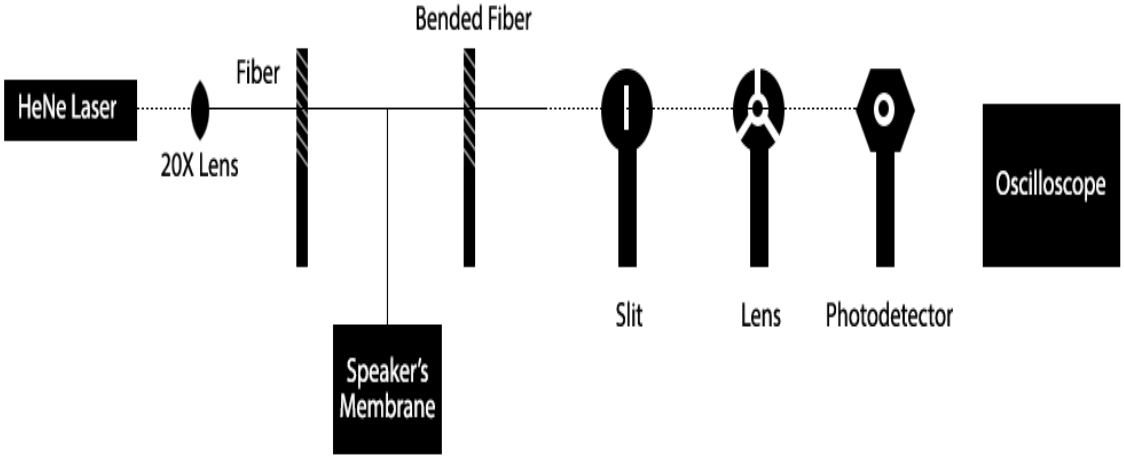

Figure 3.3. Representation of the experimental setup for vibration measurements.

In the experimental setup, firstly fiber ends are cleaved before they are placed in the light launching system to reduce the optical path difference between waveguides in the cores. To focus the laser beam into the fiber, a 20x lens is used. Linearly polarized light produced from 15mW He-Ne laser is launched into two parallel cores of the optical fiber. To obtain a good contrast of the fringe pattern, an even coupling to the cores simultaneously is significant, in the contrary case, the fringe pattern will not be clear.

Since the fiber cores are illuminated with the common laser source, guiding light in both fiber cores have a mutual coherence with each other; therefore, the fringe pattern is formed by the interference of the wave fronts from two fiber cores. Arrangement of the launch system based on the appearance of the fringe pattern is necessary to enhance the sensitivity of the system. Since the optical fiber we used has large core diameter and small core separations, higher order modes, which result in several fringe patterns occur. Bending the fiber eliminates the modes and consequently reduces the number of fringes in the interference pattern.

In our work, two fixed metal pillars as clamps shown in Figure 3.2 are used for bending the fiber, which allow obtaining a clear structured fringe pattern. When the laser beam is coupled into the two cores of the optical fiber, the fringe pattern is projected onto a slit to analyze only a desired part of the pattern to monitor on a photodetector.

The stretched fiber length between two fixed metals is about 12 cm. Vibration is applied to a point at this part of the fiber. A speaker's membrane is attached to the optical fiber (via piece of light string) and a Tone Generator that produce 100 Hz frequency sound wave are used to obtain continuous vibration in the fiber.

Vibration induced strain causes a path difference between the light beams guiding in separate cores, which result in a change in the phase of the light beam. The phase change leads to a shift in the fringe pattern. Due to the shifting of the structured light pattern, the bright fringes are replaced by the dark fringes at the slit. A photodetector behind the slit is used to detect signals derived from the variation in the phase of the light. The signals corresponding to the light intensity are related to the vibration parameters. An oscilloscope is used to record the data, which indicate the vibration amplitude and frequency.

In the next chapter, the results from the oscilloscope are shown in the figures and the signal variations are interpreted to the changes in the fringe pattern as the optical fiber vibrates.

3.3 Results for vibration

Figure 3.4 shows that the system is not stable and external factors affect the interferometric fringe pattern. As the fiber is vibrating, there are several patterns at the slit, which result in many peaks in the graph. There are sharp peaks at around 0,04V and 0,055V, therefore the bending due to vibration is causing a phase change of less than π.

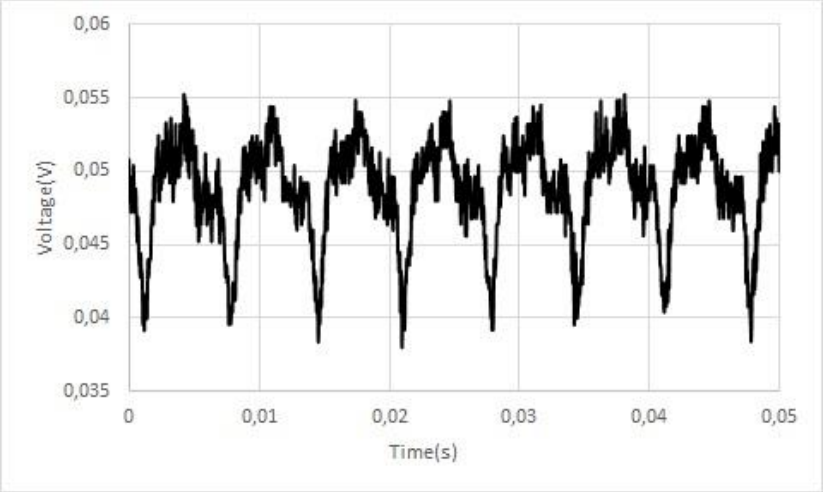

Figure 3.4. Vibration graph-1

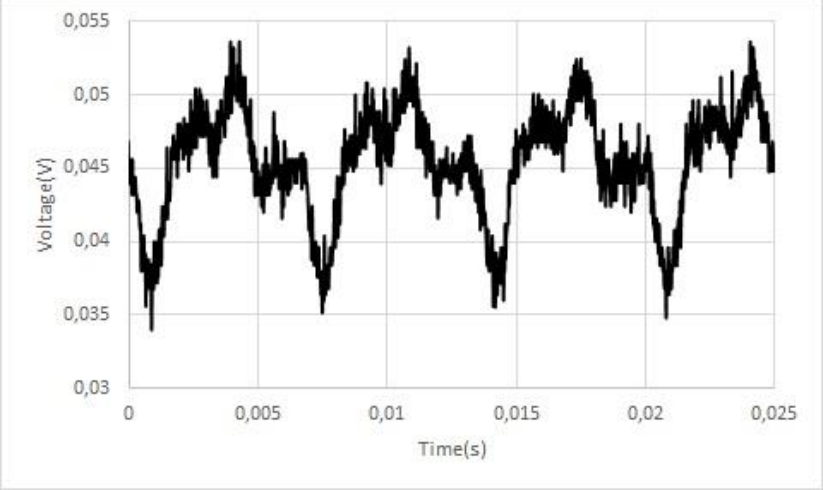

Figure 3.5. Vibration graph-2

Figure 3.5 demonstrates that when the vibration is applied to the fiber, extra patterns occur at the slit and there is a significant noise in the system. Thus, the graph does not show a regular interferometric signature and also there are sharp peaks at around 0,035V and 0,053V. This means that a phase change less than π has occurred.

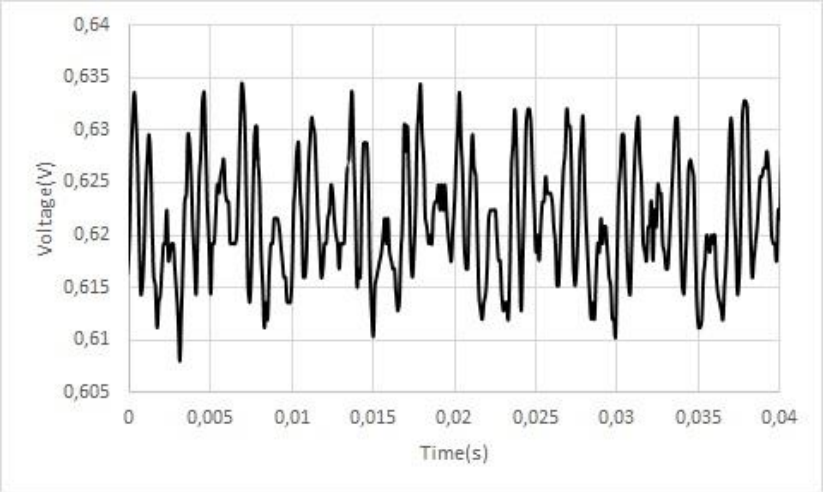

Figure 3.6. Vibration graph-3

Figure 3.6 shows that as the optical fiber is vibrating, many patterns occur at the slit which result in several peaks in the figure. There is not an exact turning point because of the sharp lines at around 0,633V, 0,630V and 0,622V. The graph does not show a regular interferometric signal. The phase change for this experimental result is also less than π.

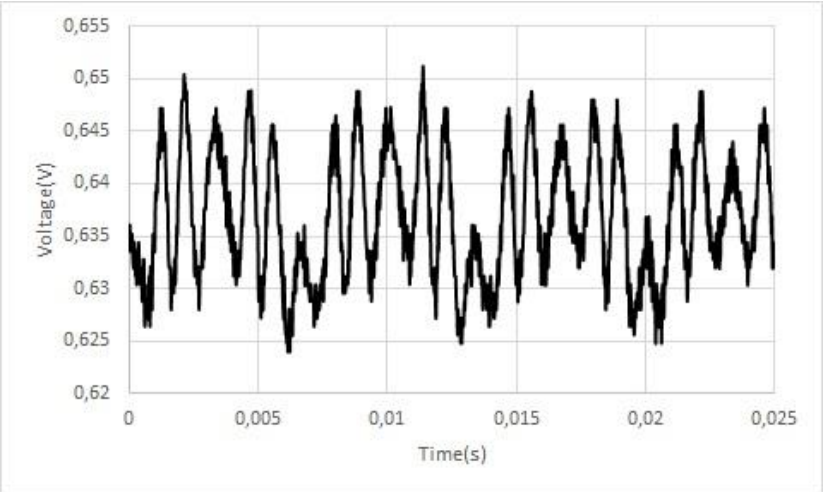

Figure 3.7. Vibration graph-4

In Figure 3.7, there are more than five peaks which means that several fringe patterns occur again at the slit during the vibration process. All peaks have sharp lines and there is not an exact turning point. The phase change due to vibration is again less than π.

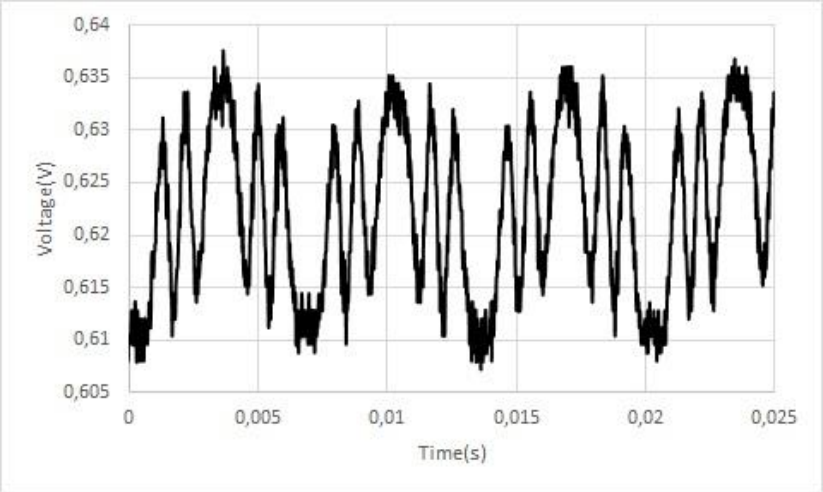

Figure 3.8. Vibration graph-5

Figure 3.8 demonstrates that there are also several patterns at the slit during the vibration, which result in many peaks. There are two turning points at around 0,635V and 0,610V. However, when the third peak at around 0,635V reaches the point at around 0,615V, sharp lines due to the other fringes interrupt the regular optical signal. Thus, the phase change is less than π.

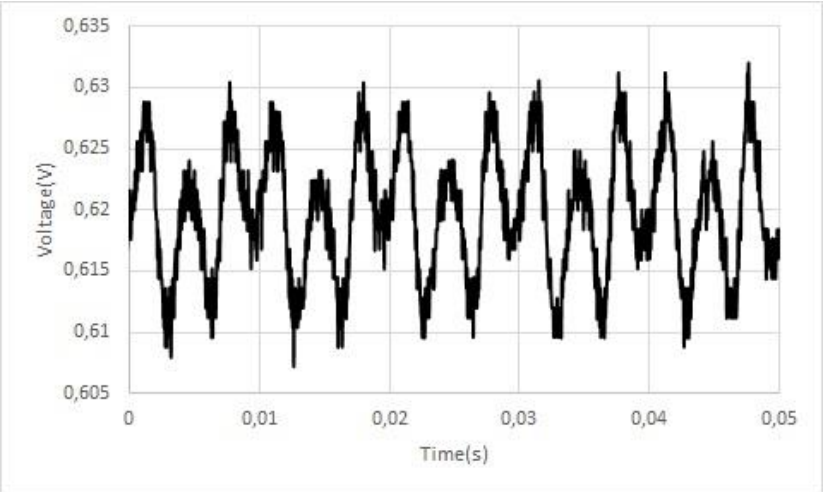

Figure 3.9. Vibration graph-6

According to Figure 3.9, at least three patterns occur at the slit, which seems to be causing by three peaks; however, only the 2nd peak seems to have reached the turning point at around 0,623V. When the second peak reaches the voltage point 0,609V, sharp peaks at around 0,61V occur and prevent a regular signal, thus a phase change due to vibration is less than π.

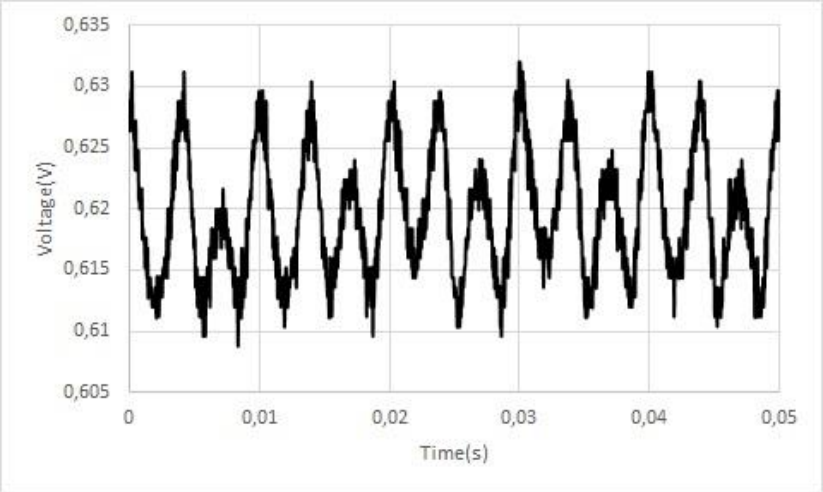

Figure 3.10. Vibration graph-7

In Figure 3.10, there are also three peaks referring to the three patterns like Figure 3.9. The second peak has a turning point at around 0,622V; but the sharp lines at around 0,630V and 0,610V are more dominant in the figure. A phase change is again less than π for this experiment.

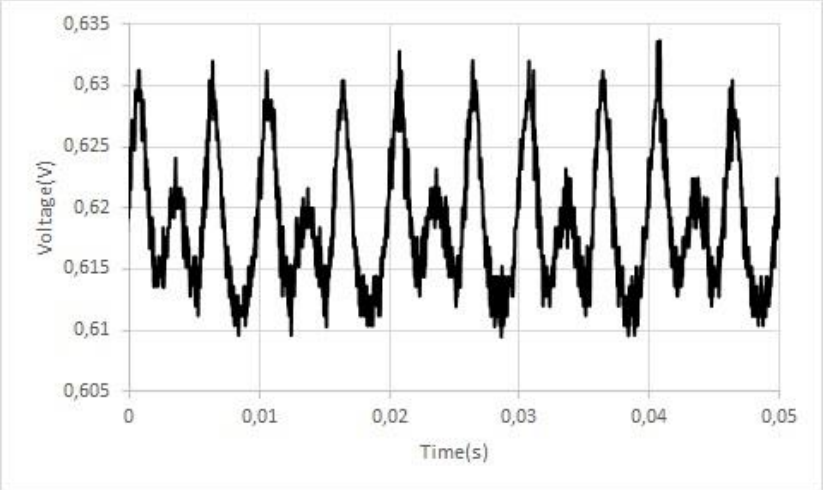

Figure 3.11. Vibration graph-8

Figure 3.11 is the same as Figure 3.10; the only difference is that the second pattern is less effective. The second pattern has a turning point at around 0,610V. It is obviously seen that when the pattern reaches the point at around 0,630V, the sharp lines occur in the figure. Thus a phase change due to vibration is less than π.

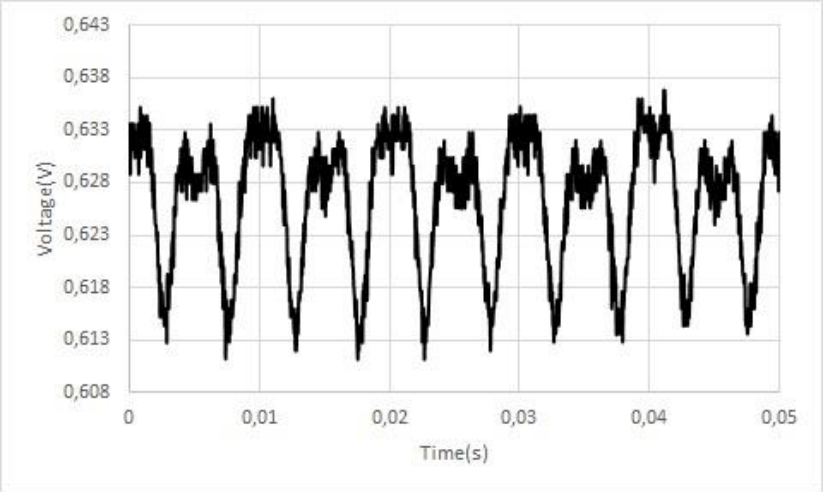

Figure 3.12. Vibration graph-9

In Figure 3.12, there are two peaks which means that at least two fringe patterns occur at the slit during the vibration. A pattern has a turning point at around 0,635V. There are sharp lines at around 0,613V. The second peak shows that the two patterns exist at the same slit at the same time. The phase change does not exceed π.

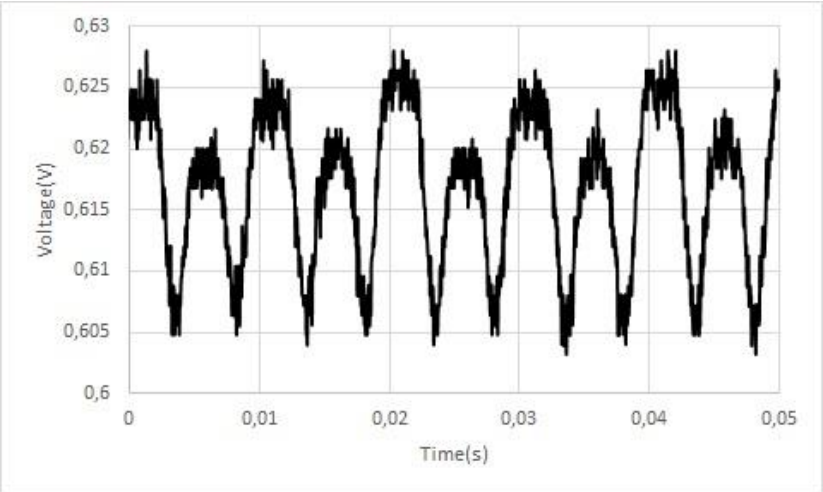

Figure 3.13. Vibration graph-10

In Figure 3.13, although there is a turning point at around 0,625V, a sharp transition occurs at 0,605V and another pattern, which has a turning point at around 0,620V emerges, thus, there is a double pattern causing two peaks in the figure. The phase change is less than π.

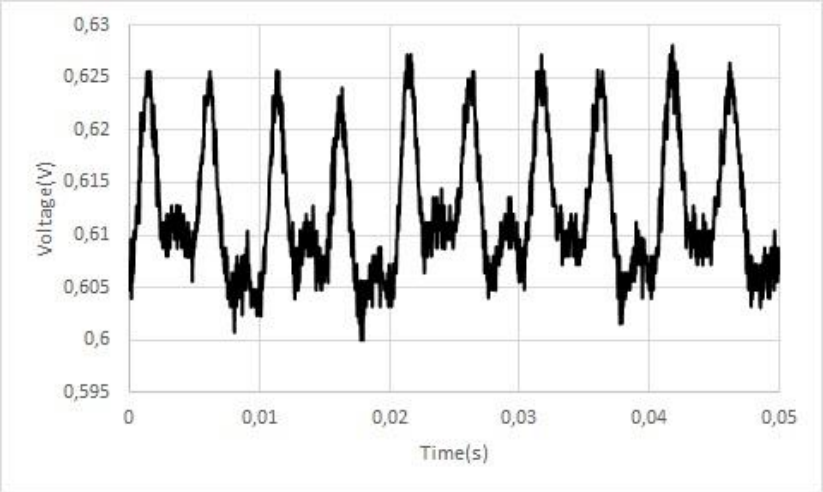

Figure 3.14. Vibration graph-11

Figure 3.14 is similar to Figure 3.13. However, the second pattern is less effective in this case. There are sharp lines at around 0,625V, which prevent a regular signal produced from a photodetector. Furthermore, the first and the second peaks demonstrate that at least two pattern exist in the slit at the same time. The phase change is less than π.

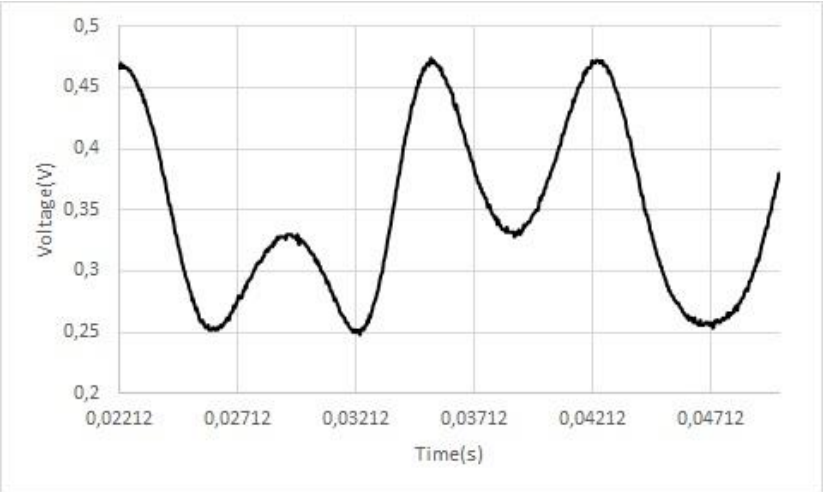

Figure 3.15. Vibration graph-12

In Figure 3.15, there is a composite fringe pattern, which result in two peaks. The first pattern is interrupted by another pattern at around 0,25V and 0,47V causing two peaks, which do not have turning points. If the second pattern does not occur at the slit, there would be a regular interferometric signal. Thus, the phase change is less than π.

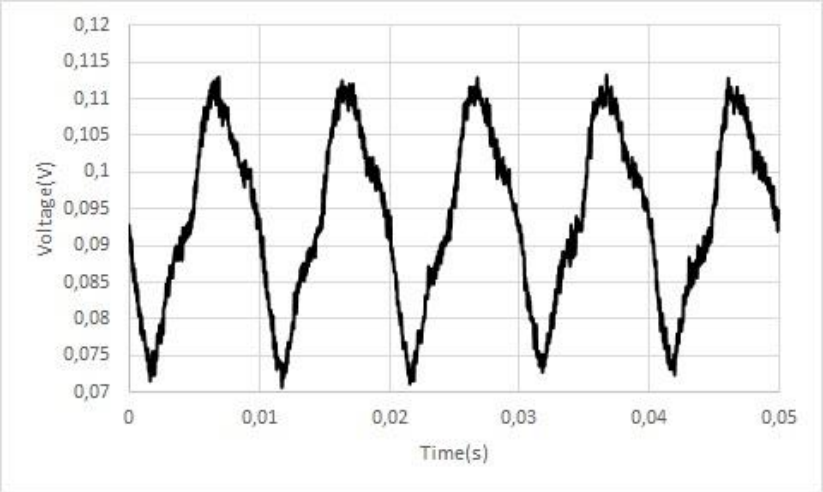

Figure 3.16. Vibration graph-13

In Figure 3.16, several fringe patterns occur at the slit. The signal from photodetector is regularly changing, but sharp transitions at the turning points at around 0,07V and 0,112V occur in the figure. Thus, the phase change is less than π.

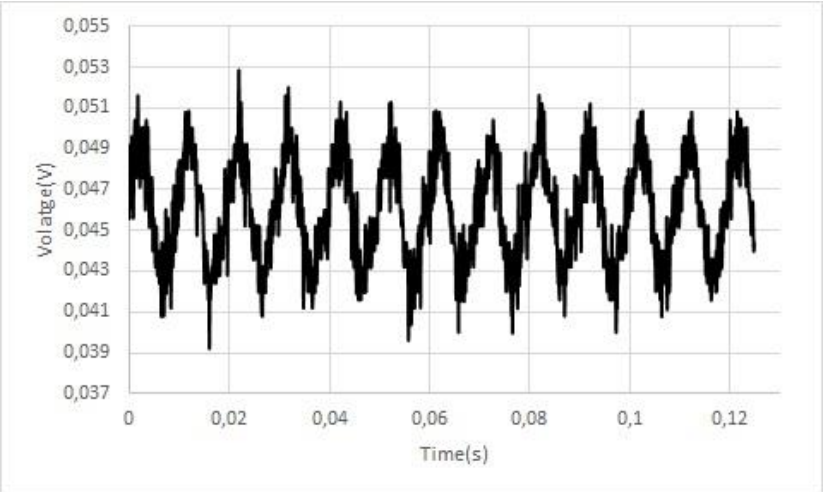

Figure 3.17. Vibration graph-14

In Figure 3.17, a single pattern is used, so the graph shows a regular interferometric signature. However, there is a significant noise, which result in sharp peaks at around 0,049V and 0,051V. The phase change is less than π.

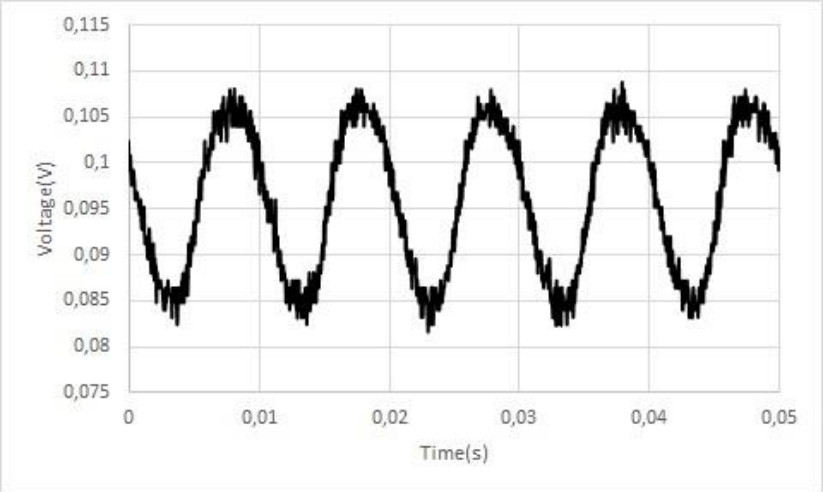

Figure 3.18. Vibration graph-15

Figure 3.18 shows that the system is stable and a single pattern causing a single peak occurs at the slit during the vibration. The peaks have exact turning points at around 0,085V and 0,108V. The graph shows a regular interferometric signature and the phase change is exactly equal to π. This means that the bright fringe at the slit is replaced by a dark fringe as the optical fiber vibrates.

According to Figure 3.18, a voltage difference of 0,020 V occurs when the phase change is equal to π. The vibration parameters are determined by analyzing the figure. The peak to peak amplitude of the vibration is equal to 0,020 V and the uncertainty of amplitude is equal to $\mp 0{,}002\ V$ and the frequency of the vibration is found by

$$f = \frac{1}{T} = \frac{1}{0{,}001\ s} = 100\ Hz \tag{3.15}$$

In addition, according to Figure 3.18, the uncertainty of frequency is equal to $\mp 2\ Hz$.

Results of the vibration sensor are presented through corresponding figures in the form of intensity versus time graphs, which are due to the phase change of the light beams propagating in each multicore-fiber. According to the figures shown in chapter 3.3, when the vibration is applied to the optical fiber, a voltage difference occurs as an indicator of vibration. However, it is hard to achieve a regular interferometric signature like that is shown in Figure 3.18. As the fiber is exposed to the vibration, coupling of the light beam into each core changes or mode interference occurs in the fringe pattern; thus, some unwanted patterns appear at the slit, which may demolish the main signal in concern. This is why we have several peaks occurring in the figures.

It is demonstrated in Figures 3.4 and 3.5 that there is a noise associated to the optical pattern during the first taken measurements. It is obvious that the fringe pattern is not stable. The following measurements represented by Figures 3.6, 3.7, and 3.8 show that there are the effects of several peaks but the associated noise is not significant when compared the previous ones. The latest results show that the number of extra unwanted fringes are reduced upon improving a more stable fringe pattern. Especially, in Figures 3.12, 3.13 and 3.14, there are two peaks, which caused by at least two fringe patterns. However, these results do not show a regular interferometric signature.

To obtain a better result, the fringe pattern and the system must be more stable and robust. Bending of the fiber at two fixed points helped eliminating interference of extra guided modes during the vibration, thus a fundamental mode corresponding to a more stable fringe pattern is obtained. In addition, since a noise or any thermal fluctuation can interrupt the signal from the exact data shown in Figure 3.5, the system must be isolated from the external effects. In Figure 3.18, although the signal is low due to the bending of the fiber, there is a regular interferometric signature. According to Figure 3.18, the exact voltage difference of 0,020 V corresponds to a phase difference of π when the vibration is applied to the fiber. Thus, with this last result one may extract the real value for the amplitude of the vibration. According to the Figure 3.18, the peak to peak amplitude of the vibration is 0,020 V and the frequency of vibration is equal to 100 Hz. Since Tone Generator that produces 100 Hz frequency sound wave is used to obtain continuous vibration in the fiber, the determined frequency of the vibration is verified.

In the experiment, even if there is a clear fringe pattern and a stable system, there is no certainty connected to the phase change of π. Although, there is a regular interferometric signal, it may be caused by shifting of small amount of the bright fringes at the slit, thus a phase change may not be equal to π exactly. To determine the real vibration amplitudes in our measurements, a bending measurement based on four-core optical fiber shown in Figure 3.19 is studied to find out how much voltage corresponds to a phase change of π exactly.

3.4. Experimental Setup for Bending

In the second part of this research project, a bending due to a small displacement is applied to the fiber to understand which voltage difference is corresponding to a phase change of π. Therefore, it will be clarified whether the voltage difference is exactly equal to a phase change of π or not when the vibration is applied to the optical fiber. The experimental setup used in the vibration sensor is rearranged to sense the bending shown in Figure 3.19.

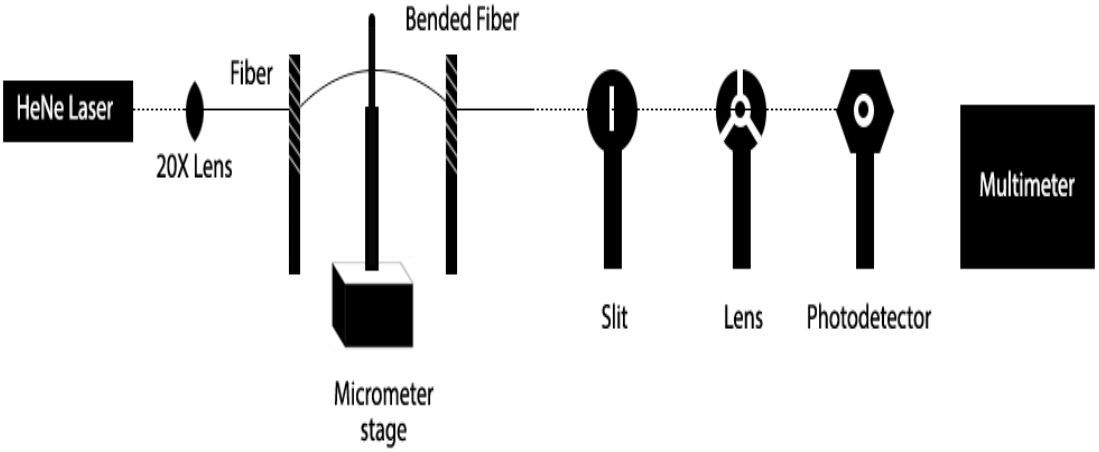

Figure 3.19. Schematic illustration of the experimental setup for bending measurements.

In the experiment, a bright line of the fringe pattern produced from a four core optical fiber is projected onto a slit. A micrometer stage is used to bend the fiber between two metals. When the displacement of the optical fiber is gradually increased, the bright line at the slit is replaced by a dark line, therefore a path difference between the cores causes a phase change of π. The signal related to the change in the intensity of the light corresponding to

the phase change is detected by a photodetector behind the slit. A multimeter is used to record the data from the photodetector.

In the next chapter, results obtained from the multimeter are presented with corresponding figures and the signal changes are interpreted according to the variation of the fringe pattern as a small displacement occurs to the stretched part of the fiber.

3.5. Results for bending

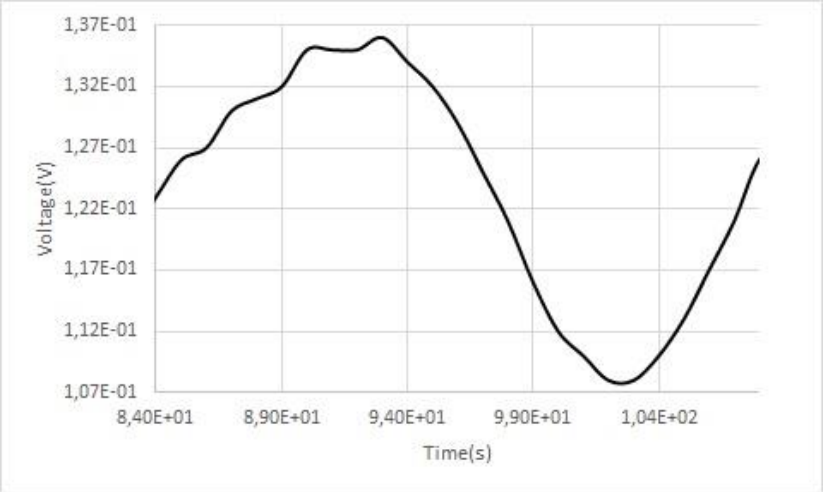

Figure 3.20. Bending graph-1

In Figure 3.20, there are two turning points at around 0,136 V and 0, 106 V, which means that when the voltage difference is 0,030 V, a phase change of π occurs. However, according to Figure 3.18, vibration induced voltage difference is 0,020 V when the phase difference is equal to π. If the measurements were taken at the same time, it may be assumed that the exact voltage difference correspond to a phase change of π is equal to 0,030 V for vibration sensor and there is not an exact shifting of the bright and dark fringes during the vibration. However, the measurements are taken at the different time. Since the system is sensitive to external conditions, when parameters are measured at different time, the position of the optical fiber may fluctuate or a coupling of the laser beam into the cores may change. Therefore, the fringe pattern used in the experiment may be different, which result in variations in voltage difference related to the phase change. In addition, because of the displacements of the micrometer stage, the lines in the graph are not smooth.

To compare the exact results of vibration and bending measurements, the results, which obtained by the same system must be used.

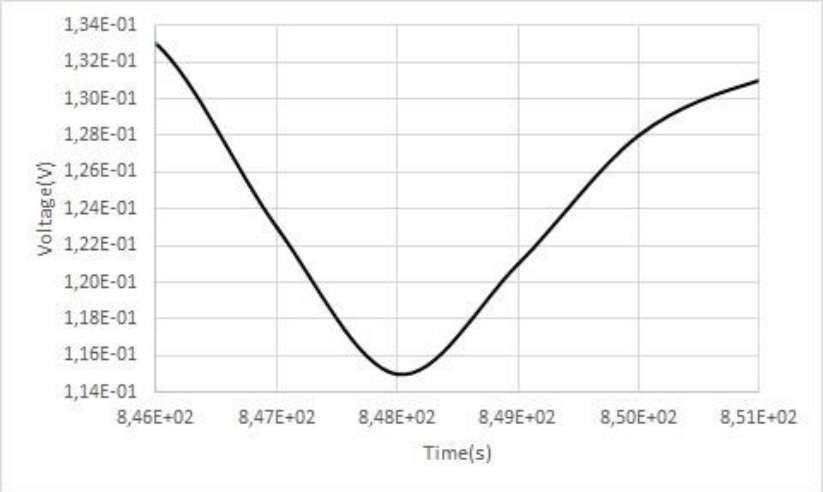

Figure 3.21. Bending graph-2

In Figure 3.21, there are turning points at around 0,133 V and 0,115 V. A phase change of π occurs when the voltage difference is approximately equal to 0,020 V. Since the bend sensing is measured at the same time with the vibration sensing, the voltage difference in the figure is approximately same as Figure 3.18. This result shows that the vibration induced voltage difference in Figure 3.18 is equal to a phase change of π.

3.6. Discussions

The main disadvantage of working with a four-core optical fiber as a vibration sensor is its sensitivity to the external factors, such as noise or thermal fluctuations. The system must be well isolated from these external effects. Firstly, to reduce the mechanical fluctuations, the optical fiber must be tense at every point in the experimental setup. The noise must be reduced as far as possible. Secondly, only a signal from the fringe pattern must be projected onto the photodetector and any light from the environment should be eliminated with an appropriate screening. In addition, the thermal fluctuations are controlled with a heat pump in the lab.

Second parameter, which affect the system's sensitivity is related to the fringe pattern used in the experimental setup. Although the four core optical fiber provides a visible interferometric fringe pattern, small core spacing with 40,6 μm and large core diameters with 10,6 μm decrease the sensitivity of the system. Since the four-core fiber used in the experiment was produced at the fiber telecommunication wavelengths of 1,3 μm and 1,55 μm, each guiding core's cutoff wavelength is higher than the operating wavelength of 632,8 nm. Thus, higher order guided modes occur in the fringe pattern, which causes the fringe pattern not being stable as the optical fiber vibrates. To overcome this problem, the modes are eliminated by bending the optical fiber. However, such a bending also decreases the signal of the light beam. When the signal is too low, a noise may occur and interrupt the exact data. Hence a four-core optical fiber with a smaller core diameter and small core spacing can be used to increase the system's sensitivity.

Finally, it is important to determine which cores are used in the experiment. When the laser beam is coupled into the two vertical or two horizontal cores, the core separation is 40,6 μm and there would be horizontal or vertical lines in the fringe pattern, which is explained in Section 2.2.2. In our experiments, two horizontal cores are used. When coupling of the laser beam into the fiber cores changes, variations occur in the fringe pattern. For an example, when the laser beam is coupled into the diagonal cores, the core separation is equal to $40{,}6\sqrt{2}$ μm. Therefore, the fringe spacing decrease.

4. CONCLUSIONS

In the first part of the thesis, our experimental work on a multi-core interferometric fiber optic vibration sensor is described. The cores of the four-core optical fiber were utilized as mutually coherent waveguides with each other; thus constituting an interference fringe pattern at the far field. Only a part of the fringe pattern is projected onto a photodetector via a single slit for precise measurements. When the vibration is applied to the optical fiber, the refractive index and length of the four-core fiber undergo a physical and optical change, which introduce a phase difference between the light beams propagating in each fiber core. As a result of such a phase change, a shift occurs in the interference fringe pattern at the far field. This shift is monitored via a single slit, which is attached to the front face of a photodetector, enabling one to relate vibration's amplitude and frequency to intensity variations of light. This type of an optical fiber sensor falls into an intrinsic sensor category, which is simple to construct and requires no need for expensive and bulky equipment, such as a spectrum analyzer.

The vibration sensor's working mechanism is based on an interferometric measurement using a four-core optical fiber. Interferometric sensors are always preferable when compared with their intensiometric counterparts since those sensors are being affected by means of any change in the source intensity, which can easily introduce errors in the measured signal. On the other hand, it is crucial to obtain a well-structured interferometric fringe pattern for healthy measurements. It is emphasized that the fringe pattern used in the experiments must be clear and highly visible since a bright part of the fringe pattern is used to monitor the phase difference. Therefore, appropriate arrangement of the launching system and handling of the optical fiber is vital to form clear fringe patterns. Furthermore, there should not be any shape variations or displacement in the fringe pattern after vibration is ceased. As the optical fiber vibrates, only the shifting of a bright line in the fringe pattern is allowed to pass through the slit and fall on the photodetector to track down the vibration induced phase change. In other words, an additional second pattern is eliminated not to occur at the slit. However, despite our efforts, this fact could not be avoided for some measurements in the beginning of our experimental work as shown in many figures in the

Experimental Part of the thesis. The optical setup is optimized carefully and a desired result is finally obtained (see Figure 3.18).

In the second part of the thesis, bending experiments are studied to determine the exact voltage difference, which is equal to a phase change of π. In the experiment, a micrometer stage is used for bending the fiber. When the displacement of the stretched part of the optical fiber occurs, a phase change of π arises from the shifting of the bright and dark fringes. Thus, a strain induced voltage difference is exactly equal to π when the voltage difference is equal to 0,020 V, which is consistent with the results presented in Figure 3.18.

In conclusion, a simple and low cost fiber optic vibration sensor, which determines vibration amplitude and frequency is accomplished in this work. For a future work, the vibration sensor maybe improved by adding temperature parameters into the measurements. Thus, a fiber optic sensor, which is capable of both sensing temperature and vibration simultaneously can be studied. It is vital to measure these two parameters at the same time for many industrial applications. It is a fact that sensors have complex structures and it is not quite simple and cheap to fabricate since the low cost may decrease the reliability of these devices. To obtain a simple and low cost sensor, intrinsic properties of the four-core optical fiber presented in our work can easily be used. When temperature is applied to the optical fiber, the change in refractive index and length of the cores lead to a phase change. Since the physical properties of the vibration and temperature are distinct, the parameters of the temperature will be different from that of the vibration ones. Thus, when the temperature and vibration is applied to the optical fiber simultaneously, their parameters will be determined separately by the same signal.

REFERENCES

1. Yoany Rodriguez Garcia, Jesus M. Corres, and Javier Goicoechea, "Vibration detection using optical fiber sensors ", *Journal of Sensors*, Vol. 2010, 2010.

2. Byeong Ha Lee, Young Ho Kim, Kwan Seob Park, Joo Beom Eom, Myoung Jin Kim, Byung Sub Rho and Hae Young Choi, "Interferometric fiber optic sensors", *Sensors*, Vol.12, pp. 2467-2486, 2012.

3. Prerana P., Varshney R. K., Pal B. P., Nagaraju B. "High sensitive fiber optic temperature sensor based on a side-polished single-mode fiber coupled to a tapered multimode overlay waveguide", *J. Opt. Soc.*, Vol.14, pp. 337-341, 2010.
4. Ferreira L.A., Ribeiro A.B.L., Santos J.L., Farahi F., "Simultaneous measurement of displacement and temperature using a low finesse cavity and a fiber Bragg grating", *Technol. Lett.,* Vol.8, pp. 1519-1521, 1996.

5. Cho J.Y., Lim J.H., Lee K.H., "Optical fiber twist sensor with two orthogonally oriented mechanically induce long-period grating sections", *Technol. Lett.,* Vol.17, pp. 453-455, 2005.

6. Wang A., Xiao H., Wang J., Wang Z., Zhao W, May R.G., "Self-calibrated interferometric-intensity-based optical fiber sensors", *J. Lightw. Techol.*, Vol.19, pp. 1495-1501, 2001.

7. Kim D.W., Shen F., Chen X., Wang A. "Simultaneous measurement of refractive index and temperature based on a reflection-mode long-period grating and an intrinsic Fabry-Perot Interferometer Sensor", *Opt.Lett.*, Vol.30, pp. 3000-3002, 2005.

8. Choi W.S., Jo M.S., "Accurate evaluation of polarization characteristics in the integrated optic chip for interferometric fiber optic gyroscope based on path-matched interferometry". *J. Opt. Soc.*, Vol.13, pp. 439-444, 2009.

9. Beard P.C., Perennes F., Draguioti E., Mills T.N., "Optical fiber photoacoustic-photothermal probe", *Opt. Lett.*, Vol.23, pp. 1235-1237, 1998.

10. Wang X., Xu J., Zhu Y., Cooper K.L., Wang A., "All-fused-silica miniature optical fiber tip pressure sensor", *Opt. Lett.*, Vol.31, pp. 885-887, 2006.

11. Bahareh Gholamzadeh, and Hooman Nabovati, "Fiber Optic Sensors", *World Academy of Science , Engineering and Technology,* Vol.2, No.6, 2008.

12. Rao Y.J., "Recent progress in fiber-optic extrinsic Fabry Perot Interferometric sensors", *Opt. Fiber Technol.*, Vol.12, pp. 227-237, 2006.

13. Tarun Kumar Gangopadhyay, "Prospects for Fibre Bragg Gratings and Fabry-Perot Interferometers in fibre-optic vibration sensing", *Sensors and Actuators A,* Vol.113, pp. 20-38, 2004.

14. Qizhen Sun, Deming Liu, Jian Wang, Hairong Liu, "Distributed fiber-optic vibration sensor using a ring Mach Zhender interferometer", *Optics Communications,* Vol.281, pp. 1538-1544, 2008.

15. Ran Z.L., Rao Y.J., Liu W.J., Liao X., Chiang K.S., "Laser-micromachined Fabry-Perot optical fiber tip sensor for high resolution temperature measurement of refractive index", *Opt.Express*, Vol.16, pg. 2252-2263, 2008.

16. H. Qu, G.F. Yan, and M. Skorobogatiy, "Interferometric fiber-optic bending/ nano-displacement sensor using plastic dual-core fiber", *Optics Letters*, Vol.39, pg. 4835-4838, 2014.

17. M.J.Gander, D. Macrae, E.A.C. Galliot, R. McBride, J.D.C. Jones, P.M. Blanchard, J.G. Burnett, A.H. Greenaway, M.N. Inci, "Two-axis bend measurement using multicore optical fibre", *Optics Communications,* Vol.182, pg. 115-121, 2000.

18. Bahaa E.A. Saleh, Malvin Carl Teich, "Fundamentals of Photonics", Wiley, New York, 1991.

19. S.O. Kasap, "Optoelectronics and Photonics" 1988.

20. Frank L. Pedrotti, S.J. Leno M. Pedrotti, Leno S. Pedrotti, "Introduction to Optics", 1987.

21. Eugene Hecht, "Optics", 2002.

22. Karahan Bulut, M. Naci Inci, "Three-dimensional optical profilometry using a four-core optical fibre", Optics Laser Technology, Vol.37, pg. 463-469, 2005.

23. R. Vallee and D. Drolet, "Practical coupling device based on a 2-core optical fiber", App. Opt., Vol.33, pg. 5602-5610, 1994.

24. S. Tunç Yılmaz, Umut D. Özuğurel, Karahan Bulut, M. Naci Inci, "Vibratiom amplitude analysis with a single frame using a structured light pattern of a four-core optical fibre", *Optics Communications,* Vol.249, pg. 515-522, 2005.

25. D.A. Jackson, "Monomode optical fibre interferometers for precision measurement", *J. Phys. E*, Vol.18, pg. 981-1001, 1985.

26. G. Meltz, W.W. Morey, W.H. Glenn, and J.D. Farina, "In-fiber Bragg-grating temperature and strain sensors", *Proceedings of the 34th International Instrumentation Symposium,* pp. 239-242, 1988.

27. G. Meltz, W.W. Morey, W.H. Glenn, and J.D. Farina, “In-fiber Bragg-grating sensors”, *Proceedings of the optical Fiber Sensors,* Vol. 2, pg. 163-166, 1988.

28. T.K. Gangopadhyay, “Prospects for Fibre Bragg gratings and Fabry-Perot interferometers in fibre-optic vibration sensing”, *Sensors and Actuators A”,* Vol.113, pp. 20-38, 2004.

29. Atsushi Wada, Satoshi Tanaka, and Nobuaki Takahashi, ”Optical fiber vibration sensor using FBG Fabry-Perot Interferometer with wavelength scanning and fourier analysis”, *IEEE Sensors Journal,* Vol.12, pg. 225-239, 2012.

30. Ivan Lujo, Pavo Klokoc, Tin Komljenovic, Marko Bosiljevac, Zvonimir Sipus, “Fiber-optic vibration sensor based on multimode fiber”, *Radioengineering”,* Vol.17, pg. 93-97, 2008.

31. P.M. Blanchard, J.G. Burnett, G.R.G. Erry, A.H. Greenaway, P. Harrison, B. Mangan, J.C.Knight, P.St.J. Russell, M.J.Gander, R. McBride and J.D.C. Jones,” Two dimensional bend sensing with a single, multi-core optical fibre”, *Smart Mater. Struct.*” Vol.9, pg. 132-140, 2000.

32. Burnett J.G., Erry G.R.G, Dickson R, McBride R., Gander M., Jones J.D.C., Blanchard P.M., Harvey A.R., and Greenaway A.H., “Channelled spectrum interrogation of an all-fibre broadband interferometric differential strain sensor fiber., *Proc. Applied Optics Divisional Conf.”* pp. 105-10, 1998.

33. Primak W. and Post D., “Photoelastic constants of vitreous silica and its elastic coefficient of refractive index”, *J. Appl. Phys.*, Vol.30, pp. 779-88, 1959.